PHYSICAL REVIEW B **70**, 155302 (2004)

Lateral confinement and band mixing in ultrathin semiconductor quantum wells with steplike interfaces

N. Shtinkov,* P. Desjardins, and R. A. Masut
Département de Génie Physique and Regroupement Québécois sur les Matériaux de Pointe (RQMP), École Polytechnique de Montréal, Case Postale 6079, Succursale "Centre-Ville," Montréal (Québec), Canada H3C 3A7

S. J. Vlaev
Escuela de Física, Universidad Autónoma de Zacatecas, Apartado Postal C-580, 98068 Zacatecas, ZAC, Mexico

(Received 5 April 2004; published 4 October 2004)

We study theoretically the effects of lateral confinement on the electronic structure of strained ultrathin InAs/InP (001) quantum wells (QWs) with one-dimensional (wirelike) interface islands. We develop a theoretical approach allowing the efficient computational treatment of a large class of one-dimensional structures within the framework of the surface Green's-function matching formalism. Using the semiempirical sp^3s^* nearest-neighbor tight-binding model, we calculate the energies, spatial distributions, and orbital character of electronic states for islands oriented along the $\langle 010\rangle$ and $\langle 110\rangle$ directions. The presence of the interface steps gives rise to localized states and leads to a band-gap reduction and an increase of the splitting between heavy holes (HH) and light holes (LH). We observe significant changes in the orbital character of both localized and extended (QW) states, namely a large anisotropy of the in-plane p components in all subbands and an increase of the p_z contribution to HH states. The valence-band structure depends strongly on the wire orientation. In $\langle 110\rangle$-oriented islands, the HH-LH mixing is significantly enhanced by the lateral potential, whereas in $\langle 010\rangle$ structures there is no evidence for such enhancement. The observed effects influence the optical properties of the structures and may cause optical anisotropy, relax some of the selection rules, and enhance the oscillator strengths for both interband and intersubband transitions.

DOI: 10.1103/PhysRevB.70.155302 PACS number(s): 73.21.Fg, 73.21.Hb

I. INTRODUCTION

Semiconductor quantum wells, wires, and dots are becoming increasingly important and already have numerous applications in microelectronic and optoelectronic devices for telecommunications and information technologies. In the past decade, the progress in growth and processing techniques has allowed us to fabricate semiconductor films as thin as a few monolayers (ML). With decreasing layer thicknesses, interfaces play an increasingly important role in determining the electronic, optical, and transport properties of the heterostructures and become of crucial importance for their suitability for device applications. The vast majority of the numerous studies on the electronic structure of semiconductor quantum wells (QWs), however, assume perfectly abrupt interfaces with only a small number being devoted to the investigation of structures with realistic interfaces. Most of the attention has been focused on theoretical investigations of the effects of interface roughness,[1–3] segregation,[3–5] and interdiffusion.[6–8] A few works have also been devoted to steplike interfaces, considering periodic steplike interface modulation with varying amplitude (step depth), leading to a quantum wirelike (one-dimensional) behavior of the confined states.[9,10] In a recent study, we have investigated the energies of the localized states arising due to lateral confinement from monolayer steps at the interfaces of thin InAs/InP QWs.[11] It has been pointed out that the presence of interface terraces leads to significant modifications of the band structure, affecting both localized and extended (QW) states. To the best of our knowledge, no detailed theoretical investigation of these effects has been carried out until now, although experimental observations have emphasized their importance in heterostructures.[12–14]

The lack of studies on this problem is partly due to its numerical complexity, since the presence of interface steps reduces the dimensionality of the structure and greatly increases the required computational effort. Envelope-function,[15,16] tight-binding,[16,17] pseudopotential,[18] and effective bond orbital[19,20] methods have been used to investigate the localized states of one-dimensional structures (quantum wires). Because the envelope-function approximation is no longer valid for structures with dimensions of several lattice constants,[21,22] one has to employ atomistic band-structure models for calculating the electronic states of ultrathin QWs. The large dimensions of the matrices involved in such calculations severely limit the possible size of the supercell and, consequently, the size of the structures that can be studied. Even larger supercells are necessary for an adequate study of the extended states, since they are strongly affected by the boundary conditions. The treatment of such large supercells is possible by means of high-performance algorithms for matrix diagonalization such as the Lanczos method.[23] These algorithms, however, compute only a limited number of well-separated eigenstates and are therefore suited only to the study of the discrete spectrum of the system (localized states). For the continuous spectrum (extended states), they quickly become impractical, since one needs to consider thousands of eigenstates in order to obtain an adequate description of the electronic structure. A theoretical approach allowing the investigation of both localized

1098-0121/2004/70(15)/155302(11)/$22.50

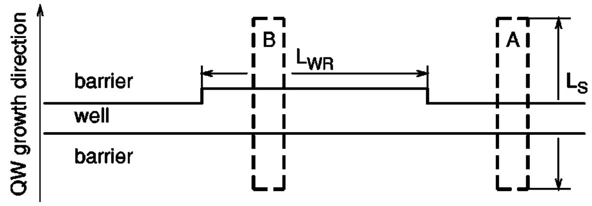

FIG. 1. A schematic plot of the structures under study. The QW interfaces are shown with a solid line, and principal layers are plotted with a dashed line. *A* and *B* denote principal layers containing QWs with different thicknesses. The structures are periodic in the direction perpendicular to the plot.

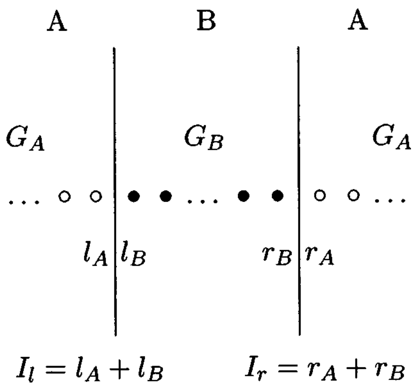

FIG. 2. Principal layer representation of the structures from Fig. 1. Each symbol represents a principal layer. *A* and *B* are the domains containing narrower (wider) QWs, respectively. The two interface domains and the four interface layers are shown with the corresponding notation.

and extended states of systems with characteristic dimensions of up to several hundreds of lattice constants will contribute to a more realistic theoretical description of quantum heterostructures, and to a better understanding of the complex relationship between the interface morphology and the electronic and optical properties of quantum heterostructures.

In Sec. II, we develop an efficient theoretical method for calculating the electronic structure of a large class of 1D structures, based on the surface Green's-function matching (SGFM) formalism.[24] We employ this approach to study the effects of one-dimensional (1D) lateral confinement of carriers in ultrathin InAs/InP (001) QWs due to monolayer steps at the QW interfaces. The electronic properties of these structures are very sensitive to monolayer width fluctuations, making them suitable test systems for studying carrier localization.[6,11–14] The details of our calculations and the geometry of the structures are outlined in Sec. III. In Secs. IV–VI we present the results of our electronic-structure calculations. The effects of the wire width and orientation on the calculated energies, spatial distributions, and orbital character of the valence- and conduction-band states are analyzed. It is demonstrated that the electronic structure of ultrathin QWs is considerably modified due to the presence of interface steps. These modifications can have important consequences on the optical properties of the structures, which are discussed in Sec. VII. We conclude in Sec. VIII with a summary of our results and a few final remarks on the possible applications of the developed theoretical approach.

II. SURFACE GREEN's-FUNCTION MATCHING FOR ONE-DIMENSIONAL SYSTEMS

We consider the effect of one-dimensional lateral confinement from interface steps (terraces) on the electronic properties of QWs within the framework of the discrete surface Green's-function matching (SGFM) formalism[24] and the empirical tight-binding (TB) method. Our model structures, sketched in Fig. 1, consist of a slab of a width L_S, containing a QW in which one of the interfaces is planar and the other exhibits two steps (terraces), delimiting a wirelike region (WR) of a width L_{WR}. The structures are periodic in the direction of the wire (perpendicular to the plot).

The SGFM method allows us to calculate the Green's function of a compound system from the Green's functions of its constituent domains. A key concept in the SGFM formalism is the *principal layer*, defined to satisfy the following two conditions:[24] (i) be a unit cell for translation perpendicular to the interfaces; (ii) couple only with adjacent (nearest-neighbor) principal layers. Note that here the term "interfaces" means interfaces between the constituent domains of the system, which are different from the QW interfaces shown in Fig. 1. The atomic details of the principal layer depend on the structure geometry (in our case, QW growth direction and wire orientation) and the underlying physical model (e.g., first- or second-nearest-neighbor method). However, these are mere technical details; in order to keep the discussion as general as possible, we define the principal layer for our systems as an atomic chain in the QW growth direction (perpendicular to the QW interfaces) satisfying the above conditions. In terms of principal layers, we now have a sandwich structure *ABA*, where *A* and *B* are domains containing QWs with different thicknesses (see Fig. 1). A schematic plot of the structures and the layer notation in the chosen principal layer representation is shown in Fig. 2. Let us denote the Green's functions of the *A* and *B* domains as G_A and G_B, and define the Green's function of the external domain G_e, consisting of the two *A* domains, as equal to G_A in each *A* domain. Using the layer notation of Fig. 2, we define the projections at the interfaces between the *A* and *B* domains $I_e = l_A + r_A$, $I_B = l_B + r_B$, and $I = I_e + I_B$. The interface projections of G_e and G_B are

$$\widetilde{G}_e \equiv \langle I_e|G_e|I_e\rangle = \begin{pmatrix} \langle l_A|G_A|l_A\rangle & 0 \\ 0 & \langle r_A|G_A|r_A\rangle \end{pmatrix}, \tag{1}$$

$$\widetilde{G}_B \equiv \langle I_B|G_B|I_B\rangle = \begin{pmatrix} \langle l_B|G_B|l_B\rangle & \langle l_B|G_B|r_B\rangle \\ \langle r_B|G_B|l_B\rangle & \langle r_B|G_B|r_B\rangle \end{pmatrix}. \tag{2}$$

Using the SGFM analysis,[24] we obtain the matrix elements of the Green's function of the entire system G_S,

$$\begin{aligned} \langle n_j|G_S|n'_j\rangle = {} & \langle n_j|G_j|n'_j\rangle + \langle n_j|G_j|I_j\rangle \widetilde{G}_j^{-1} \\ & \times (\widetilde{G}_S - \widetilde{G}_j)\widetilde{G}_j^{-1}\langle I_j|G_j|n'_j\rangle, \end{aligned} \tag{3}$$

$$\langle n_j|G_S|n'_k\rangle = \langle n_j|G_j|I_j\rangle \widetilde{G}_j^{-1}\widetilde{G}_S\widetilde{G}_k^{-1}\langle I_k|G_k|n'_k\rangle, \qquad (4)$$

where n_j denotes a principal layer of the domain j ($j=e,B$), and $j \neq k$. The full interface projection of G_S is given by[24]

$$\widetilde{G}_S^{-1} = EI - \sum_{n_e \in (e)} \langle I|H_S|n_e\rangle\langle n_e|G_e|I_e\rangle\widetilde{G}_e^{-1} - \sum_{n_B \in (B)} \langle I|H_S|n_B\rangle\langle n_B|G_B|I_B\rangle\widetilde{G}_B^{-1}, \qquad (5)$$

where H_S is the full Hamiltonian of the system. Equations (3)–(5) give exact expressions for the Green's function G_S of the compound system. Note that all operations, including the matrix inversion, should be performed in the space in which the corresponding objects are defined.

The presented approach is much more computationally efficient compared to a conventional supercell calculation. In Eqs. (3)–(5), all calculations are carried out within the subspaces of interface projections, which are 2×2 block matrices. The block size depends on the slab thickness L_S and on the size of the TB basis. The SGFM calculation time scales *linearly* (at worst) with the wire width L_{WR}, since the elements of the Green's function are computed by multiplication by the amplitude transfer matrix T (i.e., $G_{n,0}=T^nG_{0,0}$),[24] compared to a *cubic* dependence on L_{WR} for the supercell calculation. Therefore, the computation time in the SGFM method scales as $(L_{\mathrm{WR}}L_S^3)$, compared to $(L_{\mathrm{WR}}^3L_S^3)$ in the supercell approach. The advantageous scaling properties, combined with the modest memory needs due to the use of smaller matrices, allow the application of the SGFM method for the investigation of a wider array of important physics problems. The results presented in this paper are obtained for principal layers containing 40 atoms in a TB model with 10 orbitals per atom, hence we deal with 800×800 matrices. With respect to both computing time and memory requirements, this is a huge improvement over the approximately $10^5\times 10^5$ matrices needed for a supercell calculation of similar structures. In addition, once the Green's functions G_A and G_B are calculated, one may investigate systems with various widths of the wirelike region with only a small computational effort, whereas in the supercell approach one needs to diagonalize the Hamiltonian for each value of L_{WR}.

III. CALCULATION DETAILS

In our calculations of ultrathin InAs/InP (001) QWs, we have used the nearest-neighbor sp^3s^* semiempirical tight-binding (TB) model[25] with the parameters of Ref. 26, which include the spin-orbit coupling. Although more elaborate TB parametrizations are available,[27] the sp^3s^* model provides a suitable theoretical framework for our study, since it combines a satisfactory description of the band structure throughout the entire Brillouin zone with a small basis size that facilitates the computation. The on-site energies are calculated by the virtual crystal approximation, using a compositional average over the first nearest neighbors, and the two-center integrals are computed by a compositional average over the atoms entering the corresponding bonds. The unstrained valence-band offset at the InAs/InP heterojunction is taken to be 0.3 eV, which is within the accepted range of values, giving a good agreement with the experimental results.[6,28]

Strain effects are included in the Hamiltonian by scaling the two-center integrals with the bond length according to a modified Harrison's law,[29]

$$ij\kappa(d) = \left(\frac{d_0}{d}\right)^{\nu_{ij\kappa}} ij\kappa(d_0), \qquad (6)$$

where $d(d_0)$ is the strained (unstrained) interatomic distance. For the exponents $\nu_{ij\kappa}$ we use the values of Ref. 26, which are obtained by fitting the bulk deformation potentials. The on-site energies of the p orbitals E_p are modified to account for the crystal-field splitting according to[21]

$$E_p^{x,y} = E_p + b_p(\epsilon_{\parallel} - \epsilon_{\perp}),$$

$$E_p^{z} = E_p - 2b_p(\epsilon_{\parallel} - \epsilon_{\perp}), \qquad (7)$$

where $\epsilon_{\parallel}$ and $\epsilon_{\perp}$ are the in-plane and interplane components of the strain tensor, and b_p is a constant fitted in order to reproduce the deformation potential b. We have used $b_p=0.7$ eV for InAs.[21] The atomic positions in the $\langle 001\rangle$ direction are calculated using the macroscopic elasticity theory, with bulk lattice constants and elasticity moduli of InAs and InP taken from Ref. 28. In the (001) plane, the atoms are fixed at the positions of the atoms of the InP substrate, i.e., the additional strain due to the presence of interface steps is not taken into account. This approximation can be justified by recalling that strain plays a minor role in ultrathin QWs compared to confinement effects.[6] We have performed calculations of unstrained (relaxed) structures, which reveal only small quantitative changes in the calculated electronic structure. Therefore, we can expect that an exact calculation of the atomic positions, including the lateral compression, would not lead to qualitative changes in our results.

The local density of states (DOS) is calculated from the Green's function

$$N(E,n,m) = -\frac{1}{\pi}\lim_{\epsilon\to +0} \mathrm{Im}\,\mathrm{Tr}[G_{S;n,n}(E+i\epsilon)]_{m,m}, \qquad (8)$$

where E is the energy, n is the principal layer index, m is the atom index within the principal layer, $G_{S;n,n}\equiv\langle n|G_S|n\rangle$ is the diagonal element of the Green's function corresponding to principal layer n, and the trace is taken over orbitals centered at atom m (within principal layer n). We use a finite value of $\epsilon=0.001$ eV when calculating the Green's functions. The matrix elements of G_S are calculated using Eqs. (3)–(5), and the Green's functions G_A and G_B are computed using an efficient iterative algorithm.[30,31] The energies of the electronic states are derived from the interface DOS

$$\widetilde{N}(E) = -\frac{1}{\pi}\lim_{\epsilon\to +0} \mathrm{Im}\,\mathrm{Tr}[\widetilde{G}_S(E+i\epsilon)], \qquad (9)$$

i.e., the local DOS at the four layers belonging to the interface domain I, which contains the entire spectra of the structures under study.[24]

We have calculated the electronic structure of 2-ML-wide InAs/InP (001) QWs, in which one of the interfaces is planar

TABLE I. Energies of the bound states in ultrathin InAs/InP (001) QWs. The calculations are made for a 20 ML (001) slab, periodic in the $\langle 001\rangle$ direction.

QW width	E1 (eV)	HH1 (eV)	LH1 (eV)
2 ML	1.333	0.118	0.033
3 ML	1.286	0.180	0.059

and the other one exhibits two 1-ML steps, delimiting a wirelike region containing a 3-ML-wide QW. A schematic view of the structures is shown in Fig. 1. Interface terraces oriented along the $\langle 010\rangle$ or $\langle 110\rangle$ directions are considered. For $\langle 110\rangle$ structures, the p_x and p_y orbitals are equivalent due to symmetry, therefore an analysis of the orbital composition of the states in a basis with p orbitals oriented along the $\langle 100\rangle$, $\langle 010\rangle$, and $\langle 001\rangle$ directions (p_x, p_y, p_z) cannot yield information about the preferential orientation of the in-plane p components of the wave functions. In order to obtain complete information on the orbital character of the electronic states, the calculations are carried out in a basis with p orbitals oriented parallel $(p_\parallel)$ and perpendicular $(p_\perp)$ to the wire. This is achieved by the basis change $(|p_x\rangle, |p_y\rangle) \rightarrow (|p_\parallel\rangle, |p_\perp\rangle)$, where

$$\left.\begin{aligned} |p_\perp\rangle &= |p_x\rangle \\ |p_\parallel\rangle &= |p_y\rangle \end{aligned}\right\} \langle 010\rangle \text{ wires}$$

$$\left.\begin{aligned} |p_\perp\rangle &= (|p_x\rangle - |p_y\rangle)/\sqrt{2} \\ |p_\parallel\rangle &= (|p_x\rangle + |p_y\rangle)/\sqrt{2} \end{aligned}\right\} \langle 110\rangle \text{ wires.}$$

One monolayer in the $\langle 110\rangle$ direction is equal to $\sqrt{2}$ ML in the $\langle 010\rangle$ direction, therefore we will denote the $\langle 110\rangle$ length units as $\sqrt{2}$ ML. The lateral width of the wirelike region L_{WR} is varied between 2 $(2\sqrt{2})$ ML and 45 $(32\sqrt{2})$ MLfor $\langle 010\rangle$ $(\langle 110\rangle)$ wires, respectively. In all calculations, we have considered a (001) slab with periodic boundary conditions in the $\langle 001\rangle$ direction and infinite in the (001) plane. For a slab thickness of 20 ML, the change in the bound-state energies due to coupling between neighboring QWs is less than 15 meV for electrons and 10 meV for holes. Increasing the slab thickness L_S to 40 ML leads only to small quantitative changes in the calculated band structures. Since we aim to investigate the general trends rather than obtaining precise numerical results, a slab thickness of L_S=20 ML is sufficient for our purposes and has been used in the present study. The calculated energies of the electron (E), heavy-hole (HH), and light-hole (LH) states for periodic 20-ML slabs with 2- and 3-ML-wide QWs without interface steps are shown in Table I. The zero energy is at the InP valence-band edge.

IV. RESULTS: CONDUCTION BAND

A. Energy spectrum

The energies of the conduction-band states for $\langle 110\rangle$ and $\langle 010\rangle$ wires, derived from the peaks of the interface DOS $\widetilde{N}(E)$, are shown in Fig. 3. The energy spectra of the structures depend on the wire width, but remain the same for the two wire orientations, which is a direct consequence of the isotropy of the conduction band. The energy of the conduction-band ground state of the 2-ML QW (1.333 eV) divides the spectra into two parts. At energies below 1.333 eV, the spectra consist of discrete energy levels, corresponding to 1D bound states (BS). The 1D localization is driven by the lateral confining potential of 47 meV, arising from the difference between the energies of the electron states in 2-ML and 3-ML QWs (see Table I). The distributions of the local DOS (i.e., the wave function square) throughout the wire cross section are plotted in Fig. 4 for four representative cases. As can be seen from the spatial distributions of the typical first and second conduction-band BS, shown in Figs. 4(a) and 4(b), respectively, the BS are well localized in the wire region. However, at small wire widths ($L_{\mathrm{WR}} \leqslant 7$ ML) the BS energy is closer to the QW band edge and the state begins to delocalize. Its wave func-

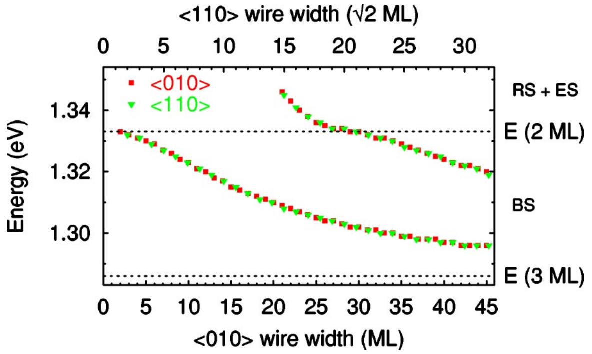

FIG. 3. (Color online) Dependence of the conduction-band bound state energies on the wire width L_{WR} for $\langle 010\rangle$ and $\langle 110\rangle$ wire orientations. The energy of the conduction-band ground states of the 2 and *3* ML QWs is shown with horizontal lines at 1.333 eV and 1.286 eV, respectively.

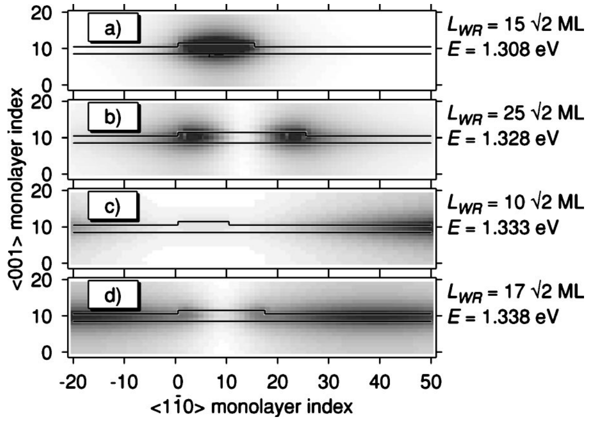

FIG. 4. Spatial distribution of the conduction-band states in $\langle 110\rangle$ wires: (a) first localized state, (b) second localized state, (c) extended state, and (d) quasilocalized state. The InAs/InP interfaces are shown with a solid line; the wire widths and the energies of the states are shown next to each figure. The intensity scale is linear, the DOS of the extended states (c) and (d) is multiplied by 8 in order to achieve a contrast level comparable to that of the bound states (a) and (b).

tion decreases rather slowly with distance, having appreciable amplitude tens of monolayers away from the wire. As we will see in the next section, this delocalization is accompanied by a modification of the states' orbital character, showing a close resemblance between the BS in narrow wires and the 2D states of the QW.

Above 1.333 eV, we observe the continuous energy spectrum of the 2D states of the 2 ML QW (not shown in the figure), projected onto the Γ point of the 1D Brillouin zone due to the reduced symmetry of the structure. These extended states (ES) are characterized by localization in the 2 -ML QW region [Fig. 4(c)]. Their amplitude in the wire region is strongly suppressed. Superimposed over the continuous spectrum, there is another set of discrete states. These are resonant states (RS), arising from the coupling of the continuous QW spectrum with the wire potential. Their spatial distribution, shown in Fig. 4(d), resembles that of ES; however, they penetrate substantially in the wire region. The RS amplitude in the wire is stronger for RS energies near the QW band edge and fades quickly at higher energies. We note that the energies of RS plotted in Fig. 3 are approximate due to the following reasons. (i) They have a small amplitude and become indistinguishable from the ES at energies higher than 1.346 eV. (ii) The energy of these states is not well determined, since they are delocalized. The energy shown in the figure is that of the peak density of states, but it should be understood that these states span a wider energy range of about 10–20 meV.

B. Orbital character

The typical 2D electron ground state of a (001) QW based on direct-gap semiconductors originates from the Γ minimum of the conduction band and is predominantly s-like, with a small (up to several percent) contribution of p_z due to the projection of the bulk states from the ⟨001⟩ Γ-X axis onto the $\overline{\Gamma}$ point of the 2D Brillouin zone. The p_x and p_y contributions are very small but nonzero, since the $p_{x,y}$ and p_z orbitals of opposite spins are weakly coupled at Γ through the spin-orbit part of the Hamiltonian.[32] In a 2-ML InAs/InP (001) QW, the orbital composition of the conduction-band state is $s/(p_x+p_y)/p_z = 96.9\%/0.34\%/2.6\%$. The orbital composition of the DOS (and, respectively, the wave functions) in the investigated wirelike structures deviates significantly from these values due to the wire potential, which breaks the symmetry of the structures. These deviations affect the symmetry of the states and can have important implications on the symmetry-related properties, such as the optical selection rules and the oscillator strengths of the optical transitions.

In order to study the effect of the interface terraces on the conduction-band states, we have calculated the percentage contributions of the s, $p_\perp$, $p_\|$, and p_z orbitals to the interface DOS $\widetilde{N}$ for the states from the discrete spectra (BS and RS). The results are plotted in Fig. 5 versus the energy of the states, for the first three states in ⟨010⟩ (⟨110⟩) wires from $2\ (2\sqrt{2})$ to $60\ (42\sqrt{2})$ ML wide. One important result from our calculations, evident from Fig. 5, is that the curves corresponding to different states practically coincide for a given wire orientation, showing that the orbital composition of the states for wires with a given orientation depends only on the energy. For BS ($E < 1.333$ eV), the curves for the first, second, and third states are identical, and the differences in the orbital character for the different RS ($E \geqslant 1.333$ eV) are less than 0.4%. Also, due to the isotropy of the conduction band, the orbital characters of the states in ⟨010⟩ and ⟨110⟩ wires are almost identical. The p_z orbital (not shown in Fig. 5) has a constant contribution of 3.6%, which does not change with the wire width and orientation.

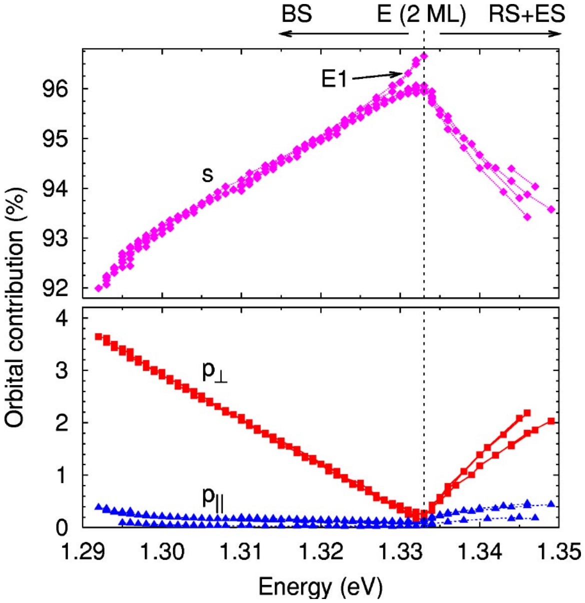

FIG. 5. (Color online) Contributions of the s, $p_\perp$, and $p_\|$ orbitals to the conduction-band local DOS in the principal layers adjacent to the interface terraces. Lines connect symbols corresponding to states with the same index (first, second, etc.) and wire orientation, but different wire widths. The energy of the 2 ML QW conduction-band edge (1.333 eV) is shown with a vertical line.

The $p_\|$ (oriented along the wire) contribution remains almost zero throughout the energy range of interest. For energies near the QW subband edge, the $p_\perp$ contribution is close to zero and the wire-induced anisotropy of the orbital character is negligible. Away from the subband edge, the states' character changes to less s-like and more $p_\perp$-like, for both BS (below 1.333 eV) and RS (above 1.333 eV). This increase is due to the loss of translational symmetry in the direction perpendicular to the wire, since the 2D band structure is projected onto the 1D Brillouin zone. Because the size quantization takes place in the direction perpendicular to the wire orientation, the $|p_\perp\rangle$ component in the wave functions increases. The results in Fig. 5 represent the orbital composition of the local DOS in the four principal layers adjacent to the interface terraces. In the wire center, the orbital character of the states approaches that of the 3-ML InAs/InP QW when increasing the wire width.

The first bound state in very narrow wires exhibits a different behavior. For $L_{\mathrm{WR}} \leqslant 7$ ML, its orbital character approaches closely that of the 2D QW state: the s contribution increases up to 96.7% (shown with an arrow in Fig. 5) and the p_z contribution decreases to 2.9%. Together with the ob-

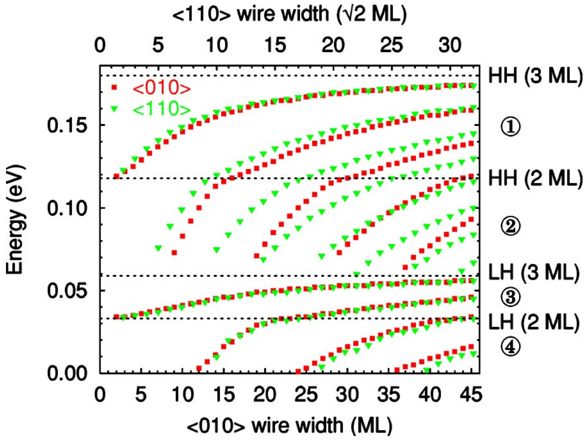

FIG. 6. (Color online) Dependence of the valence-band states energies on the wire width L_{WR} for ⟨010⟩ and ⟨110⟩ wire orientations. The energies of the HH and LH ground states of the 2 and 3 ML QWs are shown with horizontal lines and the four energy regions are marked with numbers at the right side of the graph (see the text for explanation).

served delocalization of the wave function at these wire widths, this shows that the electronic states in narrow wires are 2D-like and resemble closely the states from the QW subbands.

V. RESULTS: VALENCE BAND

A. Energy spectrum

The calculated energies of the bound states in the valence band of structures with ⟨010⟩ and ⟨110⟩ wires are shown in Fig. 6. Similarly to the conduction-band states, we can classify the states into BS, ES, and RS with respect to their spatial distributions. However, due to the presence of HH and LH subbands, the valence-band spectra are much more complex than those of the conduction band. The 1D potential couples the HH and LH states, therefore characterization of valence-band states as heavy or light hole should be done with caution.[15,17,19] However, in ultrathin InAs/InP QWs, the HH and LH ground states are well separated, therefore in Fig. 6 one can clearly distinguish the states originating from different hole subbands. Further, we will refer to these states as HH and LH according to the 2D subband of origin, but in some cases the HH-LH mixing is so strong that this notation is kept only for convenience. The energies of the HH and LH states in 2- and 3-ML QWs (shown in the figure with horizontal lines) divide the valence-band spectra of the structures into four distinct regions, and each one is characterized by a different set of states.

Region 1 ($0.180\ \mathrm{eV} > E > 0.118\ \mathrm{eV}$). For energies greater than the HH subband edge of the 2-ML QW, there are only 1D HH states localized in the wire (BS). Their spatial distributions are similar to those shown in Figs. 4(a) and 4(b).

Region 2 ($0.118\ \mathrm{eV} \geqslant E \geqslant 0.059\ \mathrm{eV}$). In this energy region, we observe extended HH states (ES) forming a continuous spectrum (not shown in the figure) and HH resonances (RS), represented by symbols in Fig. 6. Their spatial distribution is similar to that of the conduction-band states [see Fig. 4(c) for ES and Fig. 4(d) for RS].

Region 3 ($0.059\ \mathrm{eV} > E > 0.033\ \mathrm{eV}$). Between the LH subband edges of the 2- and 3-ML QWs, we observe localized LH states (BS), superimposed over a continuum of HH states. The HH resonances are not seen as peaks in the interface DOS and are not shown in the figure, however their presence can be indirectly observed in ⟨110⟩ wires and will be discussed later.

Region 4 ($0.033\ \mathrm{eV} \geqslant E \geqslant 0\ \mathrm{eV}$). Below the LH subband edge of the 2-ML QW, both HH and LH extended states are present in the spectra. The LH resonances, shown with data points in Fig. 6, have very small amplitudes, but still can be distinguished from the continuous background.

The energies of the HH states exhibit significant dependence on the wire orientation due to the highly anisotropic HH dispersion. The energies of the LH states are very close in ⟨010⟩ and ⟨110⟩ wires, reflecting the fact that the LH QW subband is almost isotropic. However, as we will see later, the spatial distributions and orbital characters of LH bound states depend significantly on the wire orientation. The comments we have made in the discussion of the conduction-band RS are equally valid for the valence-band RS. The points representing the RS in Fig. 6 actually show the maximum amplitude of a group of states spanning an energy range of 10–20 meV, superimposed over the continuous spectrum of the structures. The HH RS are shown only in the energy range 0.059–0.118 eV (region 2), where they are well pronounced. At lower energies (regions 3 and 4) they cannot be identified directly, however, as we will show later, their existence in ⟨110⟩ structures can be observed indirectly through their coupling with LH states, which has important consequences on the valence-band structure.

B. Orbital character

The zone-center HH states in a QW are typically constructed by p_x and p_y orbitals with a small contribution of p_z, whereas the LH states are composed of comparable amounts of p_x, p_y, and p_z orbitals. The s orbital contributions to the valence-band QW states are negligible. The orbital contributions to the 2-ML QW hole states are 49.7% $p_{x,y}$ and 0.4% p_z for HH; and 31.6% $p_{x,y}$ and 36.5% p_z for LH, respectively. The calculated contributions of the $p_\perp$, $p_\parallel$, and p_z orbitals to the HH states from energy regions 1 and 2 are shown in Fig. 7. Similarly to the conduction-band states, we see that the orbital character of the HH states depends only on the energy. The first localized state (HH1) for $L_{\mathrm{WR}} \leqslant 7$ ML, shown with arrows in the figure, deviates from this general trend and approaches the orbital character of the 2D QW states. It also begins to delocalize, showing that for narrow wires the effect of the wire potential on the electronic structure is minor and both the conduction- and valence-band ground states resemble the states from the QW subbands.

It is evident from Fig. 7 that the wire potential causes a strong anisotropy of the in-plane p component of the HH states. The latter are composed predominantly of $p_\parallel$ orbitals, followed by $p_\perp$ and a small contribution of p_z. The $p_\perp/p_\parallel$ anisotropy is much stronger for wires in the ⟨110⟩ direction.

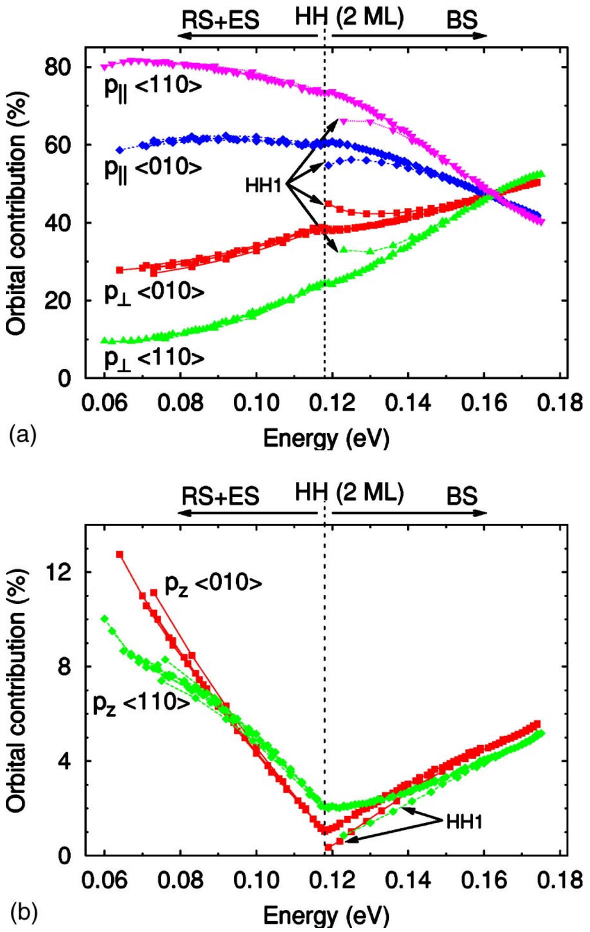

FIG. 7. (Color online) Orbital contributions to the local DOS of the HH states at the principal layers adjacent to the interface terraces: (a) $p_\perp$ and $p_\parallel$ orbitals, (b) p_z orbital. Symbols corresponding to states with the same index (first, second, etc.) and wire orientation, but different wire widths, are connected with lines. The energy of the HH band edge of the 2 ML QW (0.118 eV) is shown with a vertical line.

For $E > 0.160$ eV, the $p_\perp$ contribution becomes dominant, however this is an interface effect caused by the quicker decay of the $p_\parallel$ amplitude away from the wire center. In the wire center, the same trend of equalizing the $p_\parallel$ and $p_\perp$ contributions with increasing L_{WR} takes place, but the dominant orbitals remain $p_\parallel$ for all considered values of L_{WR}. The HH states have the smallest p_z contribution (or, in other words, they are most HH-like) when they are close in energy to the HH band edge of the QW [see Fig. 7(b)]. Away from the QW band edge, the p_z contribution increases and can reach almost 6% for BS and 12% for RS.

We have performed a similar analysis for the LH states. Unlike the electrons and heavy holes, the orbital character of the LH states strongly varies between states with similar energies because they are superimposed on a continuous background from HH extended states with varying amplitude. Other reasons for the observed differences are the spatial variations of the orbital composition of the QW LH states due to strain[33] and the mixing between LH and HH states that we will investigate in the following section. The LH bound states (region 3) are typically composed of $p_\perp$ orbitals (around 45%), followed by $p_\parallel$ (around 35%) and p_z (around 20%). The in-plane anisotropy is again more pronounced in ⟨110⟩ wires; besides, for this wire orientation the variations of the states' orbital character with the wire width and the energy are much larger. In region 4, we observe a marked dependence of the orbital character of the RS on the wire orientation: in ⟨010⟩ wires, the states are similar to the LH BS with a dominant $p_\perp$ contribution, whereas in ⟨110⟩ wires the $p_\parallel$ component prevails. The p_z contribution to the states in this energy region is smaller in ⟨110⟩ structures (10–15 %), compared to ≈20% in ⟨010⟩ wires. These differences are a signature of stronger HH-LH coupling in ⟨110⟩-oriented wires and demonstrate that the states we have denoted as LH resonances are more LH-like in ⟨010⟩ and more HH-like in ⟨110⟩ wires.

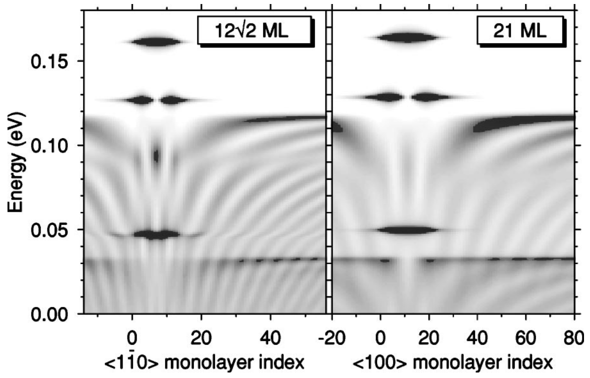

FIG. 8. Valence-band local density of states in the InAs layer for ⟨010⟩ (right) and ⟨110⟩ (left) wires. The wires start from monolayer index 1. The intensity scale is linear. The DOS is normalized to the unit area of the wire cross section.

C. Band mixing

In order to get further insight into the nature of the hole states and the coupling between the hole subbands, we have investigated the evolution of the valence-band local density of states with the energy. The results for $12\sqrt{2}$ ML ⟨110⟩ and 21 ML ⟨010⟩ wires are presented in Fig. 8. Each horizontal line in the figure represents the spatial variation of the local DOS in the InAs layer in the direction perpendicular to the wire and parallel to the QW interfaces, for that given energy. In the figures one can clearly identify the first and the second localized HH states at approximately 0.160 eV and 0.127 eV, respectively. At $E \leqslant 0.118$ eV, one finds the HH extended states continuum, originating from the projection of the HH subband of the 2-ML QW in the $k_\perp$ direction onto the 1D Brillouin zone center.

At a fixed energy, we observe a horizontal oscillating pattern in the extended states' DOS. These oscillations are due to the coupling of the ES with the wire potential. Let us recall that the ES are *extended* in the 1D context, but originate from the *localized* states of the 2D QW with a 2D in-plane wave vector $(k_\perp, 0)$ and an energy $E(k_\perp, 0)$. In the absence of a wire, the ES wave functions are plane waves $\exp(\pm i k_\perp \xi)$, where ξ is the lateral coordinate perpendicular to the wire. The local DOS (wave function squared) of these states is constant with ξ. In the presence of a wire, the plane waves scatter from the wire interfaces. The interference between the scattered waves gives rise to an interference pattern, which we observe through the DOS oscillations with ξ. The period of the oscillations $2\pi/k_\perp$ decreases with decreasing energy (i.e., increasing $k_\perp$) and is different for the two wire orientations due to the anisotropic dispersion of the 2D HH subband.

In both structures, one can observe a HH resonance around 0.090 eV, with a maximum amplitude in the wire center and two side maxima near the wire interfaces. The strong coupling between the RS and the HH continuum is evidenced by the smearing of the ES interference pattern, observed tens of monolayers away from the wire. The peak corresponding to the first localized LH state is located at $\approx$0.05 eV. While in the $\langle 010\rangle$ wire this peak bears the characteristics of a regular bound state, in the $\langle 110\rangle$ structure it has two important features: (i) it has a highly irregular shape with two maxima; and (ii) it introduces long-range changes in the ES interference pattern outside the wire. Both are signatures of strong coupling with HH states at the same energy. This coupling can be observed for all wire widths, as evidenced by the variation of the local DOS in the direction perpendicular to the wire for the first localized LH states in $\langle 110\rangle$ wires, shown in Fig. 9(a). The irregular shape of the peak suggests that the LH state is mixed with a HH resonance; in the figure one may follow the index of this RS by counting the number of peaks in the wire region. Thus we may identify the second ($L_{\mathrm{WR}}=3$ to $6\sqrt{2}$ ML), third (7 to $9\sqrt{2}$ ML), fourth (10 to $13\sqrt{2}$ ML), fifth (14 to $19\sqrt{2}$ ML), sixth (20 to $23\sqrt{2}$ ML), seventh (24 to $26\sqrt{2}$ ML), eighth (27 to $31\sqrt{2}$ ML), and ninth (32 to $34\sqrt{2}$ ML) HH states. These ranges of wire widths correspond to the values of L_{WR} for which the corresponding HH state would have energy close to the first LH state. One can easily verify this by continuing the imaginary lines representing the dependence of each HH state's energy on L_{WR} in Fig. 6 until they cross the line corresponding to the first LH state. This confirms that the irregular shape of the LH bound states in $\langle 110\rangle$ wires is due to coupling with HH resonances. We note that a similar effect has been observed in V-shaped $\langle 110\rangle$ quantum wires, where the calculated wave function of the LH-like ground state has two maxima due to coupling with HH-like localized states.[15]

For comparison, we have also calculated the spatial variation of LH states in $\langle 010\rangle$ wires [Fig. 9(b)]. It is seen from the figure that the peaks remain regular for all wire widths. For this wire orientation, there is also a small oscillating component from the HH continuum. However, as seen in Fig. 8, the LH BS is visible only in the vicinity of the wire, and the phase of the HH ES oscillations around 0.05 eV remains unchanged. This means that, contrary to the $\langle 110\rangle$ structures, the DOS at this energy is simply a superposition between LH BS and HH ES—no additional coupling between HH and LH subbands due to the wire potential takes place. These observations remain true for all wire widths and for all states in region 3: the localized LH states mix strongly with HH states in $\langle 110\rangle$ wires, while no evidence of such mixing is observed in $\langle 010\rangle$ structures.

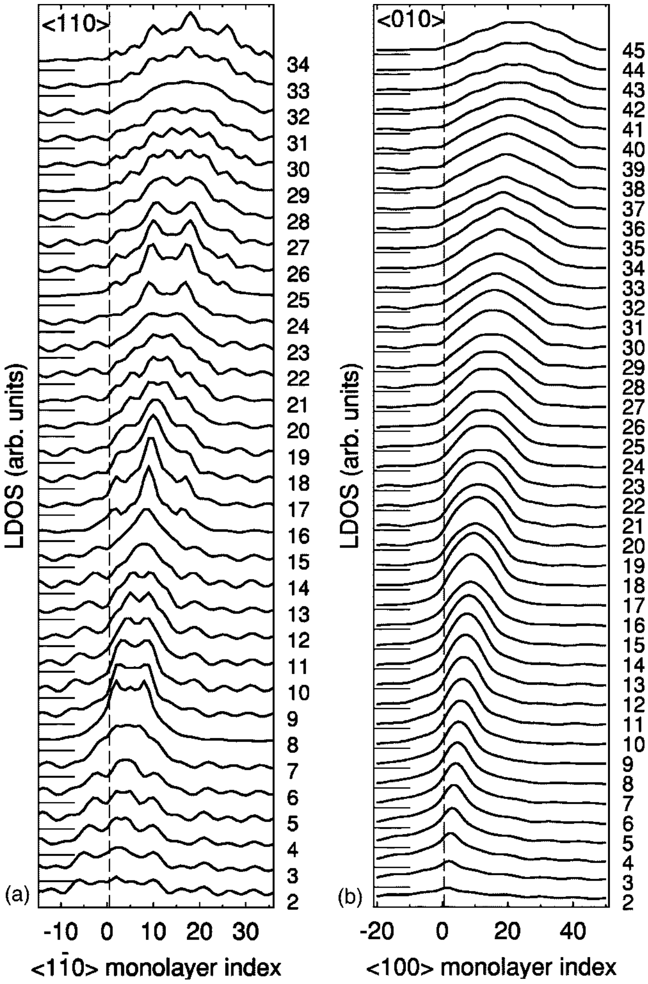

FIG. 9. Variation of the local DOS in the InAs layer for the first LH state for $\langle 110\rangle$ (a) and $\langle 010\rangle$ (b) wires. The curves are shifted horizontally for clarity; the zero of each curve is shown with a horizontal line on the left-hand side of the graphs. The wire widths are shown at the right side of the graphs in monolayers (ML for $\langle 010\rangle$ and $\sqrt{2}$ ML for $\langle 110\rangle$). The vertical dashed line shows the left interface of the wire.

At energies below 0.033 eV (region 4), one observes in Fig. 8 the LH extended states originating from the $k_\perp$ projection of the LH subband of the 2 ML QW. Again, there is a pronounced difference between the two wire orientations. In the $\langle 010\rangle$ structure, the LH ES show a similar interference pattern to the HH states, superimposed on the HH continuum. In contrast, the LH states in $\langle 110\rangle$ wires show no visible oscillations. The ES DOS in this energy region is dominated by the spatial oscillations characteristic of the HH states, confirming our conclusion based on the analysis of the orbital contributions that the states in this energy region are of predominantly HH character in $\langle 110\rangle$ wires.

VI. OTHER STRUCTURE GEOMETRIES

In the structures investigated so far, the two interface steps occur at the same QW interface, forming a wirelike interface island (see Fig. 1). Such islands can be obtained

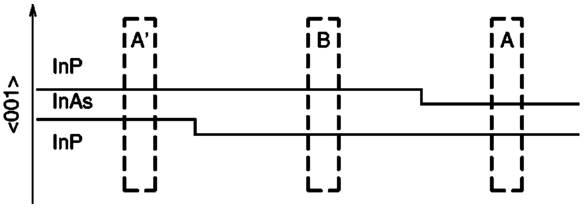

FIG. 10. Schematic plot of (001) InAs/InP QWs grown on misoriented substrates. The InAs/InP interfaces are shown with a solid line. The principal layers corresponding to the three different domains A', B, and A are shown with a dashed line.

unintentionally during epitaxial growth of QWs. In Fig. 10, we have shown a different structure geometry, in which the two consecutive 1-ML steps that delimit the wirelike region occur at the opposite QW interfaces. Such structures are more likely to be formed during growth on misoriented substrates. In principal layer representation, we again have a "sandwich" sequence of 2 ML/3 ML/2 ML QWs, however in this case the left and right semi-infinite domains A and A' are nonequivalent from a geometry point of view (see Fig. 10). The SGFM analysis of the $A'BA$ system remains essentially the same, the only difference being that in this case we define G_e as equal to $G_{A'}$ in the left and to G_A in the right semi-infinite domain. Using this definition, the application of the SGFM formulas described in Sec. II is straightforward.

The electronic structure of systems with $A'BA$ geometry closely resembles that of ABA systems having the same wire width and orientation. Our calculations reveal small quantitative differences (typically below 1%) in the local DOS between the two structure geometries. The maximum differences are found inside the wire region at energies near the LH localized states and are around 3% for $\langle 010\rangle$ and 6% for $\langle 110\rangle$ structures. Besides these small modifications of the local wave-function amplitude, the calculated energies, spatial distributions, and orbital character of the electronic states in ABA and $A'BA$ systems are essentially identical. Therefore, all results presented in the previous two sections are also valid for the structures shown in Fig. 10.

We have also calculated the electronic structure of 1-ML and 3-ML InAs/InP (001) QWs, containing 2-ML and 4-ML InAs wires, respectively. The impact of the interface islands on the QW electronic structure is stronger for thinner QWs, because the lateral confining potential is greater. For the same reason, the HH-LH mixing is also enhanced in thinner QWs, and in 1-ML QWs a significant valence-band mixing is observed for the $\langle 010\rangle$ wire orientation as well.

VII. DISCUSSION

The results presented in the previous sections demonstrate that the electronic structure of 2-ML InAs/InP (001) QWs is profoundly influenced by the presence of 1D (wirelike) interface islands. This influence is manifested by the appearance of bound states, localized in the wirelike regions, with energies up to 30 meV below the QW subband edge for electrons, 50 meV above the QW subband edge for HH, and 20 meV for LH states. Thus, the presence of interface islands leads to an increased HH-LH splitting and to a band-gap reduction of up to 80 meV. Having in mind that we consider lateral localization in only one dimension, we find that the experimentally measured difference of 50 meV between the energies of the free and localized HH excitons in 2-ML InAs/InP QWs with 3-ML interface islands[14] is in good agreement with our calculations. In order to carry out a more precise comparison of our results with experimental data, one would need a specially fabricated sample with preferential island orientation and a certain uniformity in the island dimensions, which so far has proven difficult to achieve.

The orbital character of the localized states exhibits significant deviations from the 2D QW states. A great anisotropy of the in-plane p components is observed in both the conduction and the valence band. For electron bound states, we find an increase of the $p_\perp$ component up to ten times while the p_z and $p_\parallel$ components remain almost constant. The HH (LH) states are composed predominantly by $p_\parallel$ $(p_\perp)$ orbitals, and the p_z contribution to the HH states increases significantly with respect to the QW states. The valence-band structure exhibits a marked dependence on the wire orientation. While in structures with $\langle 010\rangle$-oriented wires we found no evidence for significant enhancement of the HH-LH coupling, in $\langle 110\rangle$ structures we have observed very strong HH-LH mixing, virtually leading to the absence of pure LH states in these systems. The different HH-LH coupling in $\langle 110\rangle$ and $\langle 010\rangle$ wires is probably a consequence of the different symmetry of the structures. A group-theoretical discussion of the symmetry effects in 1D structures with different shapes and crystallographic orientations can be found in Refs. 34 and 35.

An interesting aspect of our findings is the large in-plane anisotropy of the HH states and its dependence on the wire orientation. A recent study has identified the origins of the in-plane anisotropy in 2D (001) zinc-blende structures as (i) asymmetry of the two interfaces (e.g., in no-common-atom superlattices); and (ii) reduced symmetry in the $\langle 001\rangle$ direction (e.g., in trilayer superlattices).[36] The presence of a wirelike interface island has a twofold effect on the symmetry of the structure: it breaks the translational periodicity in the lateral direction (which naturally leads to in-plane anisotropy), and it renders the two (001) interfaces nonequivalent. The latter results in an in-plane anisotropy with principal axes [110] and $[\bar{1}10]$.[36] Thus, one can expect the difference between the in-plane p components due to the interface asymmetry to be maximal in a basis oriented along the principal axes and zero in a basis rotated at 45° with respect to them. Therefore, the smaller $p_\parallel/p_\perp$ anisotropy in $\langle 010\rangle$ wires is due only to coupling with the 1D wire potential, which breaks the lateral periodicity of the QW. The same effect takes place in $\langle 110\rangle$ wires; however, according to the above argument, the interface asymmetry leads to additional anisotropy in these structures. As demonstrated in Ref. 36, this effect is strongest for the HH states and negligible in the conduction band, which is in agreement with our results.

The effect of the interface steps on the electronic properties of the structures is not limited to carrier localization. The wire potential affects also the QW extended states and gives rise to resonant states in the QW continuum, which exhibit similar changes in their orbital character. These changes in the electronic structure of QWs with steplike interfaces can significantly affect the QW's optical properties. The selection rules and oscillator strengths in semiconductor quantum wires have been investigated theoretically for both interband[15,19] and intersubband[37] transitions. Since the BS are typical 1D states, they will exhibit similar behavior to the quantum-wire bound states; among the expected changes of the optical properties are the breakdown of the 2D selection rules due to the appearance of 1D states and a significant optical anisotropy, as confirmed by many theoretical[15,19,37] and experimental[15,38] studies on quantum wire structures. However, contrary to the quantum wire case where the transitions between localized states are of primary interest, in QWs with steplike interfaces the transitions involving extended states are equally important.

The optical properties of QWs with perfect interfaces are determined by the optical transitions between the QW states from the center of the 2D Brillouin zone. Here we will present a simplified qualitative discussion of the optical properties of QWs with steplike interfaces, based on our analysis of the orbital character of the electronic states and on an analogy with perfect QWs. We consider two cases of practical importance: the conduction-band intersubband transitions and the band-to-band transitions. In the envelope-function approximation, the Γ-point transition between the conduction subbands of n-doped (001) QWs is forbidden for normal-incident (x- or y-polarized) light (TE) and allowed for z-polarized light (TM).[39] In a tight-binding representation, the x and y components of the momentum operator, which are responsible for the TE transition, can be calculated from the TB Hamiltonian.[40] It can be shown that in a 2D (001) QW they have nonzero matrix elements only between two states with the following symmetries: s-p_x, s-p_y, p_x-p_z, and p_y-p_z. Therefore, the oscillator strength of the TE transition between two s-like electron states is zero. The small p_z contribution to the conduction-band states due to confinement in the $\langle 001\rangle$ direction also does not contribute to the TE transitions since the momentum matrix element between s and p_z is zero, and so is the one between p_z and p_z. The oscillator strength of the TE intersubband transition in n-type QWs is small but nonzero in a spin-dependent TB model due to the nonzero $p_{x,y}$ contributions to the zone-center states.[41] According to our detailed analysis of the conduction-band states in QWs with steplike interfaces, the oscillator strength of the TE transition is likely to increase in these structures due to the larger $p_\perp$ contribution to the QW extended states.

A similar analysis can be applied to the electron–heavy-hole (E-HH) interband transitions for z-polarized light. The z component of the 2D momentum matrix in (001) QWs is nonzero only between two states with s-s, s-p_z, p_x-p_x, p_x-p_y, p_y-p_y, or p_z-p_z symmetries. Following the same argument as in the previous paragraph, we see that the E-HH zone-center transition for z-polarized light is very weak in perfect (001) QWs, because the electron state is s-like and the HH state is $p_{x,y}$-like. Thus, the oscillator strength of this transition is primarily due to (i) the nonzero $p_{x,y}$ contributions to the electron (coupling to the large HH $p_{x,y}$ components), and (ii) the nonzero p_z contribution to the HH states (coupling to the large electron s component). Therefore, we can expect that the observed large increase of these (usually very small) contributions to the E and HH extended states in the investigated structures will increase the oscillator strength of the E-HH transition. Both the interband and intersubband optical spectra in QWs with steplike interfaces can be precisely calculated using the developed Green's-functions approach for 1D structures and the existing methods for computing the optical conductivity from the Green's functions of QWs with perfect interfaces.[41]

VIII. CONCLUSION

We have developed a general theoretical approach allowing the computationally efficient treatment of 1D systems in the surface Green's-function matching framework. Using the developed method and the semiempirical sp^3s^* TB model, we have investigated the effects of 1D lateral confinement on the electronic structure of ultrathin InAs/InP (001) QWs with steplike interfaces. Our results show that the electronic structure of QWs is profoundly influenced by the presence of 1D (wirelike) interface islands. This influence is manifested by the appearance of bound states, localized in the wirelike regions, with energies in the gap, thus leading to a band-gap reduction and an increase of the HH-LH splitting. The orbital character of these states exhibits significant deviations from the QW states, with an increase of the nominally negligible $p_\perp$ component for electrons and the p_z component for heavy holes. In the valence band, the coupling to the wire potential modifies the in-plane p components of the hole wave functions, increasing the $p_\parallel$ contribution to the HH and the $p_\perp$ contribution to the LH states. We found that the valence-band mixing depends on the wire orientation. In $\langle 110\rangle$-oriented wires, the HH and LH states are strongly coupled by the wire potential and no pure LH states can be observed. In contrast, the HH and LH states in $\langle 010\rangle$ islands are relatively well defined and we found no evidence for enhancement of the valence-band mixing due to the presence of interface terraces in these structures.

The effect of the wire potential on the electronic properties of the structures is not limited to the localized states. It affects also the QW extended states and gives rise to resonant states in the QW continuum, which exhibit changes in their orbital character similar to those of localized states. The observed changes in the electronic structure affect the optical properties of the structures and may cause optical anisotropy, relax some of the selection rules, and enhance the oscillator strengths for both interband and intersubband transitions due to the appearance of localized states and the changes in the orbital character of the extended states.

As a final comment, we emphasize that the use of the developed Green's-function approach is not restricted to electronic-structure calculations, or to systems with the considered "sandwich"-like geometry. It can be applied to all cases where the description of the physical problem is possible in terms of discrete matrices in principal layer representation. An example of practical interest is that of lattice vibrations, where the dynamical equation may be translated in the form of the "Hamiltonian matrix" formalism.[24] The developed approach can also be used in conjunction with the SGFM formalism for systems with N interfaces,[42] systems containing inhomogeneous parts,[43] and periodic systems (superlattices),[44,45] which allows applications to virtually any system with planar interfaces in a principal layer representation. Therefore, the developed approach is a powerful and flexible tool, providing a computationally efficient formalism for the investigation of a wide class of one-dimensional systems.

ACKNOWLEDGMENTS

The authors gratefully acknowledge the financial support of the Natural Sciences and Engineering Research Council of Canada during the course of this research. P.D. also acknowledges support from the Canada Research Chair Program.

---

*Electronic address: nshtinkov@polymtl.ca

[1] K. M. Hong, P. C. K. Kwok, and P. C. Chui, Solid State Commun. **107**, 483 (1998).
[2] I. Morrison, L. D. L. Brown, and M. Jaros, Phys. Rev. B **42**, 11 818 (1990).
[3] B. Koiller, R. B. Capaz, and H. Chacham, Phys. Rev. B **60**, 1787 (1999).
[4] R. Magri and A. Zunger, Phys. Rev. B **65**, 165302 (2002).
[5] L.-W. Wang, A. Franceschetti, and A. Zunger, Phys. Rev. Lett. **78**, 2819 (1997).
[6] N. Shtinkov, P. Desjardins, and R. A. Masut, Phys. Rev. B **66**, 195303 (2002).
[7] B. Koiller, A. S. Martins, and H. Chacham, Appl. Phys. Lett. **69**, 2423 (1996).
[8] S. J. Vlaev and D. A. Contreras-Solorio, J. Appl. Phys. **82**, 3853 (1998).
[9] T. G. Dargam, R. B. Capaz, and B. Koiller, Braz. J. Phys. **29**, 834 (1999).
[10] T. G. Dargam, R. B. Capaz, and B. Koiller, Phys. Rev. B **64**, 245327 (2001).
[11] N. Shtinkov, P. Desjardins, and R. A. Masut, Microelectron. J. **34**, 459 (2003).
[12] P. Paki, R. Leonelli, L. Isnard, and R. A. Masut, Appl. Phys. Lett. **74**, 1445 (1999).
[13] A. G. Steffan and R. T. Phillips, Physica E (Amsterdam) **17**, 15 (2003).
[14] P. Paki, R. Leonelli, L. Isnard, and R. A. Masut, J. Vac. Sci. Technol. A **18**, 956 (2000).
[15] F. Vouilloz, D. Y. Oberli, M.-A. Dupertuis, A. Gustafsson, F. Reinhardt, and E. Kapon, Phys. Rev. B **57**, 12 378 (1998).
[16] A. Di Carlo, S. Pescetelli, A. Kavokin, M. Vladimirova, and P. Lugli, Phys. Rev. B **57**, 9770 (1998).
[17] Y. Arakawa, T. Yamauchi, and J. N. Schulman, Phys. Rev. B **43**, 4732 (1991).
[18] A. Franceschetti and A. Zunger, Phys. Rev. B **52**, 14 664 (1995).
[19] D. S. Citrin and Y. C. Chang, Phys. Rev. B **43**, 11 703 (1991).
[20] L.-X. Li and Y.-C. Chang, J. Appl. Phys. **84**, 6162 (1998).
[21] M. Di Ventra and K. A. Mäder, Phys. Rev. B **55**, 13 148 (1997).
[22] R. C. Iotti, L. C. Andreani, and M. Di Ventra, Phys. Rev. B **57**, R15 072 (1998).
[23] C. Lanczos, J. Res. Natl. Bur. Stand. **45**, 255 (1950).
[24] F. García-Moliner and V. R. Velasco, *Theory of Single and Multiple Interfaces* (World Scientific, Singapore, 1992).
[25] P. Vogl, H. P. Hjalmarson, and J. D. Dow, J. Phys. Chem. Solids **44**, 365 (1983).
[26] C. Priester, G. Allan, and M. Lannoo, Phys. Rev. B **37**, 8519 (1988).
[27] J.-M. Jancu, R. Scholz, F. Beltram, and F. Bassani, Phys. Rev. B **57**, 6493 (1998).
[28] I. Vurgaftman, J. R. Meyer, and L. R. Ram-Mohan, J. Appl. Phys. **89**, 5815 (2001).
[29] W. A. Harrison, *Electronic Structure and the Properties of Solids* (W. H. Freeman and Co., San Francisco, 1980).
[30] M. P. López-Sancho, J. M. López-Sancho, and J. Rubio, J. Phys. F: Met. Phys. **14**, 1205 (1984).
[31] M. P. López-Sancho, J. M. López-Sancho, and J. Rubio, J. Phys. F: Met. Phys. **15**, 851 (1985).
[32] D. J. Chadi, Phys. Rev. B **16**, 790 (1977).
[33] G. Armelles and V. R. Velasco, Phys. Rev. B **54**, 16 428 (1996).
[34] M. A. Dupertuis, E. Martinet, D. Y. Oberli, and E. Kapon, Europhys. Lett. **52**, 420 (2000).
[35] M.-A. Dupertuis, D. Marti, and F. Michelini, Phys. Status Solidi B **234**, 329 (2002).
[36] L. C. Lew Yan Voon, Appl. Phys. Lett. **70**, 2446 (1997).
[37] D. M. Gvozdić and A. Schlachetzki, J. Appl. Phys. **94**, 5049 (2003).
[38] M. Saraydarov, V. Donchev, K. Germanova, X. L. Wang, S. J. Kim, and M. Ogura, J. Appl. Phys. **95**, 64 (2004).
[39] G. Bastard, *Wave Mechanics Applied to Semiconductor Heterostructures* (Les Éditions de Physique, Les Ulis, 1988).
[40] L. C. Lew Yan Voon and L. R. Ram-Mohan, Phys. Rev. B **47**, 15 500 (1993).
[41] N. Shtinkov and S. J. Vlaev, Phys. Status Solidi B **241**, R11 (2004).
[42] L. Fernández-Alvarez, G. Monsivais, S. Vlaev, and V. R. Velasco, Surf. Sci. **369**, 367 (1996).
[43] S. Vlaev, V. R. Velasco, and F. García-Moliner, Phys. Rev. B **49**, 11 222 (1994).
[44] M. C. Muñoz, V. R. Velasco, and F. García-Moliner, Phys. Rev. B **39**, 1786 (1989).
[45] S. J. Vlaev, I. Rodríguez-Vargas, L. M. Gaggero-Sager, and V. R. Velasco, Surf. Sci. **554**, 245 (2004).